Supporting Information

Effects of side-chain length of non-fullerene acceptors on performance in all-small-molecule organic solar cells

Fangfang Huang,[a] *Lingxian Meng,*[a] *Changzun Jiang,*[a] *Huazhe Liang,*[a] *Yang Yang,*[b] *Jian Wang,*[b] *Xiangjian Wan,*[a] *Chenxi Li,*[a] *Zhaoyang Yao,*[a] *Yongsheng Chen.*[a,*]

[a]*State Key Laboratory and Institute of Elemento-Organic Chemistry, The Centre of Nanoscale Science and Technology and Key Laboratory of Functional Polymer Materials, Renewable Energy Conversion and Storage Center (RECAST), College of Chemistry, Nankai University, Tianjin, 300071, China.*

[b]*The Institute of Seawater Desalination and Multipurpose Utilization, Ministry of Natural Resources (Tianjin), Tianjin 300192, P. R. China.*

Content

1. Materials and Synthesis

All reactions and manipulations were carried out under argon (Ar) atmosphere with use of standard Schlenk techniques. All starting materials and solvent were purchased from commercial sources without any purification unless stated otherwise. The central core (compound **1**) with two *n*-octyl was synthesized according previous reports.[1-3]

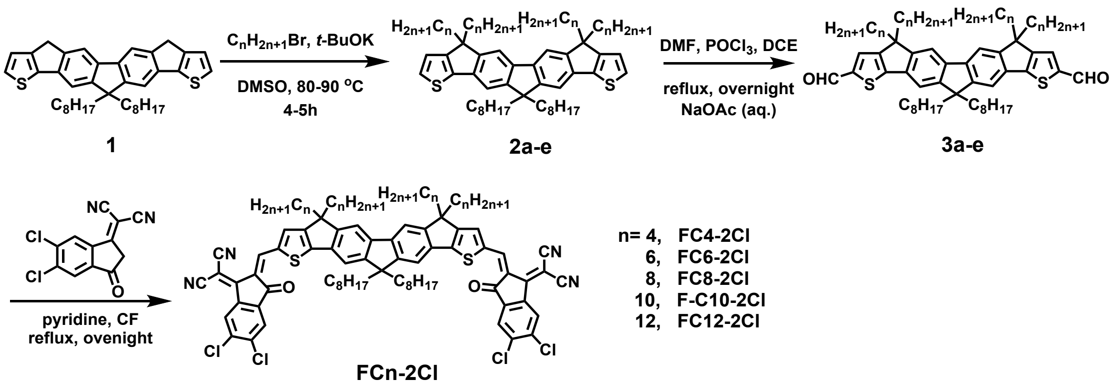

Scheme S1. The synthetic route of **FCn-2Cl** (n=4, 6, 8, 10, 12).

*General procedure for the synthesis of compound **2***

A solution of compound **1** (0.29 g, 0.50 mmol) in dry DMSO (20 mL) was heated at 80 °C. Sodium tert-butoxide (0.56 g, 4.99 mmol) dissolved in dry DMSO (15 ml) was added to the above mixture. After the reaction mixture was stirred at 80 ºC for 1 h, alkyl bromide (4.00 mmol) was added dropwise. The mixture was further stirred at 90 ºC for 4 h. After cooling to room temperature, the reaction was quenched by water and extracted with ethyl ether (30 ml × 3) and brine (50 ml × 3). After being dried over $MgSO_4$, the organic layer was removed by reduced pressure and the residue was simply purified by column chromatography on silica gel (petroleum ether) to afford sticky yellow product. The excess alkyl bromide and the product are difficult to separate, we did a crude NMR characterization and MS characterization, and then the products would be used for the next step. The excess alkyl bromide does not affect the next reaction.

*General procedure for the synthesis of compound **3***

$POCl_3$ (0.18 mL) was added drop by drop to DMF (2 mL) at 0 °C under the protection of argon and then stirred at 0 °C for 1 h. And then, the reaction flask was moved to room temperature and stirred another 4 h to gain the Vilsmerier reagent. The Vilsmerier reagent was added into a 1,2-dichloroethane (30 mL) solution of compound **1** (0.41 mmol). The above reaction mixture was stirred at room temperature for 1 h and then heated to 80 °C overnight. The mixture was cooled to room temperature and quenched with saturated CH_3COONa (aq.), and then extracted with CH_2Cl_2 (50 mL×3). The combined organic layer was dried over anhydrous Na_2SO_4 and purified by silica gel (petroleum ether/dichloromethane = 1/1, *v*/*v*) to yield product.

3a: bright yellow solid (78%) ^1H NMR (400 MHz, $CDCl_3$, δ): 9.92 (s, 2H), 7.66 (s, 2H), 7.66 (s, 2H), 7.48 (s, 2H), 2.13-2.03 (m, 8H), 1.97-1.89 (m, 4H), 1.19-0.85 (m, 40H), 0.76 (t, 18H). ^{13}C NMR (100 MHz, $CDCl_3$, δ): 183.0, 155.5, 154.9, 152.3, 151.4, 144.9, 141.0, 136.1, 130.6, 115.1, 114.0, 54.8, 54.0, 40.5, 38.9, 31.7, 29.8, 29.7, 29.2, 29.1, 26.6, 23.7, 23.1, 22.6, 14.0, 13.9. MS (MALDI-TOF): calculated for $C_{57}H_{78}O_2S_2$ [M^+], 858.54; found: 858.55.

3b: bright yellow solid (77%) ^1H NMR (400 MHz, $CDCl_3$, δ): 9.91 (s, 2H), 7.65 (s, 4H), 7.47 (s, 2H), 2.12-2.03 (m, 8H), 1.97-1.90 (m, 4H), 1.13-0.86 (m, 56H), 0.76 (t, 18H). ^{13}C NMR (100 MHz, $CDCl_3$, δ): 183.0, 155.5, 154.9, 152.3, 151.4, 141.1, 136.1, 130.6, 115.1, 114.0, 54.8, 54.0, 40.5, 39.0, 31.9, 31.8, 31.5, 29.9, 29.7, 29.6, 29.2, 29.1, 24.3, 23.7, 22.5, 14.0, 13.9. MS (MALDI-TOF): calculated for $C_{65}H_{94}O_2S_2$ [M^+], 970.67; found: 970.76.

3d: bright yellow solid (80%) ^1H NMR (400 MHz, $CDCl_3$, δ): 9.91 (s, 2H), 7.65 (s, 2H), 7,64 (s, 2H), 7,47 (s, 2H), 2.12-2.02 (m, 8H), 1.95-1.87 (m, 4H), 1.18-0.88 (m, 88H), 0.84 (t, 12H), 0.77 (t, 6H). ^{13}C NMR (100 MHz, $CDCl_3$, δ): 182.9, 155.5, 155.0, 152.3, 151.4, 144.9, 141.0, 136.1, 130.6, 115.1, 114.0, 54.8, 54.0, 40.5, 39.0, 31.9, 31.8, 30.1, 29.9, 29.7, 29.6, 29.5, 29.4, 29.3, 29.2, 29.1, 24.5, 22.6, 22.6, 14.1, 14.0. MS (MALDI-TOF): calculated for $C_{81}H_{126}O_2S_2$ [$M+H^+$], 1195.92; found: 1195.93.

3e: bright yellow solid (78%) ^1H NMR (400 MHz, $CDCl_3$, δ): 9.91 (s, 2H), 7.66 (s, 2H), 7.65 (s, 2H), 7.47 (s, 2H), 2.12-2.03 (m, 8H), 1.95-1.88 (m, 4H), 1.20-1.04 (m, 104H), 0.85 (t, 12H), 0.77 (t, 6H). ^{13}C NMR (100 MHz, $CDCl_3$, δ): 182.9, 155.5, 152.3, 151.4, 144.9, 141.0, 136.1, 130.6, 115.1, 114.0, 54.8, 54.0, 40.5, 39.0, 31.9, 31.8, 30.1, 29.9, 29.6, 29.4, 29.3, 29.2, 29.1, 24.5, 23.7, 22.7, 22.6, 14.1, 14.0. MS (MALDI-TOF): calculated for $C_{89}H_{142}O_2S_2$ [$M+H^+$], 1308.23; found: 1308.10.

General procedure for the synthesis of compound ***FCn-2Cl***

Under the atmosphere of argon, compound **3** (0.09 mmol) and **2ClIC** (0.08 g, 0.31 mmol) were dissolved in dry $CHCl_3$ (15 mL), and then pyridine (0.20 mL) was added to the mixture. After stirring and refluxing overnight, the mixture was cooled to room temperature and partial solvent was removed under vacuum. The residue was added into 50 mL methanol dropwise. The precipitate was collected and further purified by silica gel using $CHCl_3$ as eluant to afford **FCn-2Cl.**

FC4-2Cl: dark blue solid (73%) ^{1}H NMR (600 MHz, $CDCl_3$, δ): 9.01 (s, 2H), 8.78 (s, 2H), 7.96 (s, 2H), 7.76 (s, 2H), 7.72 (s, 2H), 7.66 (s, 2H), 2.16-2.06 (m, 8H), 2.00-1.95 (m, 4H), 1.22-0.84 (m, 40), 0.77 (t, 18H). ^{13}C NMR (150 MHz, $CDCl_3$, δ): 186.1, 163.5, 158.6, 157.2, 156.7, 152.6, 142.9, 140.6, 139.5, 139.4, 139.3, 138.9, 138.6, 136.6, 126.9, 125.1, 120.3, 116.5, 114.7, 114.5, 68.8, 54.8, 54.2, 40.4, 39.0, 31.8, 31.7, 29.9, 29.2, 29.1, 26.7, 23.9, 22.6, 14.1, 13.9. HR-MS: calculated for $C_{81}H_{82}Cl_4N_4O_2S_2$ $[M+H]^+$, 1350.44710; found: 1350.4740.

FC6-2Cl: dark blue solid (76%) ^{1}H NMR (600 MHz, $CDCl_3$, δ): 9.00 (s, 2H), 8.78 (s, 2H), 7.96 (s, 2H), 7.75 (s, 2H), 7.72 (s, 2H), 7,66 (s, 2H), 2.15-2.09 (m, 8H), 2.01-1.96 (m, 4H), 1.16-0.84 (m, 56H), 0.77 (t, 18 H). ^{13}C NMR (150 MHz, $CDCl_3$, δ): 186.1, 163.6, 158.6, 157.2, 156.7, 152.2, 142.9, 140.6, 139.5, 139.4, 139.3, 138.6, 136.7, 136.1, 126.9, 125.1, 120.3, 116.5, 114.7, 114.5, 68.8, 54.8, 54.3, 40.4, 39.1, 31.8, 31.5, 29.9, 29.6, 29.2, 29.2, 24.4, 23.9, 22.6, 22.5, 14.1, 14.0. HR-MS: calculated for $C_{89}H_{98}Cl_4N_4O_2S_2$ $[M+H]^+$, 1461.5929; found: 1461.5988.

FC10-2Cl: dark blue solid (76%) ^{1}H NMR (600 MHz, $CDCl_3$, δ): 9.01 (s, 2H), 8.79 (s, 2H), 7.96 (s, 2H), 7.76 (s, 2H), 7.71 (s, 2H), 7.66 (s, 2H), 2.15-2.06 (m, 8H), 1.99-1.94 (m, 4H), 1.24-1.08 (m, 88H), 0.82 (t, 12H), 0.78 (t, 6H). ^{13}C NMR (150 MHz, $CDCl_3$, δ): 186.1, 163.5, 158.6, 157.2, 156.8, 152.6, 142.9, 140.6, 139.5, 139.3, 139.3, 138.6, 136.6, 136.1, 126.9, 125.1, 120.3, 116.5, 114.7, 114.5, 68.8, 54.8, 54.2, 40.4, 39.1, 31.9, 31.8, 30.0, 29.6, 29.5, 29.4, 29.3, 29.2, 22.6, 22.5, 14.1, 14.0. HR-MS: calculated for $C_{105}H_{130}Cl_4N_4O_2S_2$ $[M+H]^+$, 1686.8466; found: 1686.8459.

FC12-2Cl: dark blue solid (76%) ^{1}H NMR (600 MHz, $CDCl_3$, δ): 9.01 (s, 2H), 8.79 (s, 2H), 7.96 (s, 2H), 7.76 (s, 2H), 7.71 (s, 2H), 7.65 (s, 2H), 2.14-2.07 (m, 8H), 1.98-1.93 (m, 4H), 1.26-0.88 (m, 104), 0.84 (t, 12H), 0.78 (t, 6H). ^{13}C NMR (150 MHz, $CDCl_3$, δ): 186.1, 163.5, 158.6, 157.2, 156.8, 152.6, 142.8, 140.6, 139.5, 139.4, 139.3, 138.7, 136.6, 136.1, 126.9, 125.1, 120.3, 116.5, 114.7, 114.5, 68.8, 54.8, 54.2, 40.4, 39.1, 31.9, 31.8, 30.0, 29.6, 29.5, 29.4, 29.3, 29.2, 22.7, 22.6, 14.2, 14.1. HR-MS: calculated for $C_{113}H_{146}Cl_4N_4O_2S_2$ $[M+H]^+$, 1798.9718; found: 1798.9690.

The compounds **2c**, **3c**, and **FC8-2Cl** have been reported and characterized in previous literatures.[1-3]

2. Instruments and Measurements

The ^1H, ^{13}C nuclear magnetic resonance (NMR) spectra were taken on Bruker AV400 and AV600 Spectrometers. Matrix assisted laser desorption/ionization time-of-flight (MALDI-TOF) were performed on a Bruker AutoflexIII LRF200-CID instrument and the High-Resolution Mass Spectra (HR-MS) were carried out on Bruker Solarix scimax MRMS instrument. The thermogravimetric analysis (TGA) was performed on a NETZSCH STA 409PC instrument under N_2 flow. The heating rate for TGA is 10 °C min^{-1}. Ultraviolet-visible (UV-*vis*) absorption spectra were performed on a UV-*vis* instrument Agilent Cary 5000 UV-*vis*-NIR spectrophotometer. Cyclic voltammetry (CV) experiments of target compounds thin films were carried out to evaluate the energy levels with a LK98BII Microcomputer based Electrochemical Analyzer in acetonitrile solution at room temperature. The experiments were recorded in a conventional three-electrode configuration with a saturated calomel electrode (SCE) as the reference electrode, a glassy carbon electrode as the working electrode and a Pt wire as the counter electrode. Tetrabutylammonium phosphorous hexafluoride (Bu_4NPF_6, 0.1M) in anhydrous acetonitrile solution was used as the supporting electrolyte with the scan rate of 100 mV s^{-1} under the protection of argon. Atomic force microscope (AFM) measurements were performed using Dimension Icon, Bruker in ScanAsyst mode. The transmission electron microscopy (TEM) investigation was performed on Phillips Technical G2 F20 at 200 kV. (GIWAXS) measurement was measured at Xenocs/Xeuss 2.0. All samples were deposited on the silicon and were irradiated at a fixed X-ray incident angle of 0.2° with an exposure time of 1800 s. The hole and electron mobility were measured using the space charge limited current (SCLC) method, employing a diode configuration of ITO/PEDOT:PSS/active layer/MoO_3/Al for hole-only devices and glass/ITO/ZnO/active layer/PDINO/Al for electron-only devices by taking the current density in the range of 0-10 V and fitting the result to space charge limited form, where SCLC is described by:

$$J = \frac{9\varepsilon_0\varepsilon_r\mu_0 V^2}{8L^3}$$

where J is the current density, ε_0 is the permittivity of free space (8.85×10^{-12} F m^{-1}), ε_r is the relative dielectric constant of transport medium, μ is the hole or electron mobility, V ($=V_{appl}-V_{bi}$) is the internal voltage due to the device, where V_{appl} is the applied voltage to the device and V_{bi} is the built-in voltage due to the relative work function difference of the two electrodes, L is the film thickness of the active layer.

The current density-voltage (J-V) characteristics of photovoltaic devices were obtained using a Keithley 2400 source-measure unit. The photocurrent was measured under illumination simulated 100 mW cm^{-2} AM 1.5G irradiation using SAN-EI XES-70S1 solar simulator, calibrated with a standard Si solar cell. The EQE spectrum was measured using a QE-R Solar Cell Spectral Response Measurement System (Enli Technology Co., Ltd., Taiwan).

TPV and TPC measurements. A white light bias was generated from an array of diodes (Molex 180081-4320) with light intensity about 0.5 sun. A diode pumped laser (Lapa-80) was used as the perturbation source, with a pulse duration of 10 ns and a repetition frequency of 20 Hz. Voltage and current dynamics were recorded on a digital oscilloscope (Tektronix MDO4104C), and voltages at open circuit and currents under short circuit conditions were measured over a 1 MΩ and a 50 Ω resistor, respectively.

3. Device Fabrication

The OSCs devices were fabricated using a conventional structure of ITO/PEDOT:PSS/Active layer/PDINO/Al. The indium tin oxide (ITO)-coated glass substrates were cleaned by ultrasonic treatment in detergent, deionized water, acetone, and isopropyl alcohol under ultrasonication for 15 min each and subsequently dried by an argon blow. Subsequently, a thin layer of PEDOT:PSS was spin-coated on top of precleaned ITO substrates at 4300 rpm for 20 s and annealed in air at 150 °C in air for 15 min. Then the **BSFTR:FCn-2Cl** (1:0.8, *w*/*w*, D: 8 mg/mL, no additives) in chloroform (CF) was spin coated at 1700 rpm to form an active layer with a thickness of 110 nm. Then the substrates were TA treatment with 120 °C for 10 min. After that, about 15 nm PDINO layer was spin coated on the top of the active layer at 3000 rpm. Finally, a layer of Al with thickness of 90 nm was thermally evaporated under a shadow mask with a base pressure of ca. 10^{-5} Pa. The active area of the device was 4 mm^2.

4. Figures and Tables

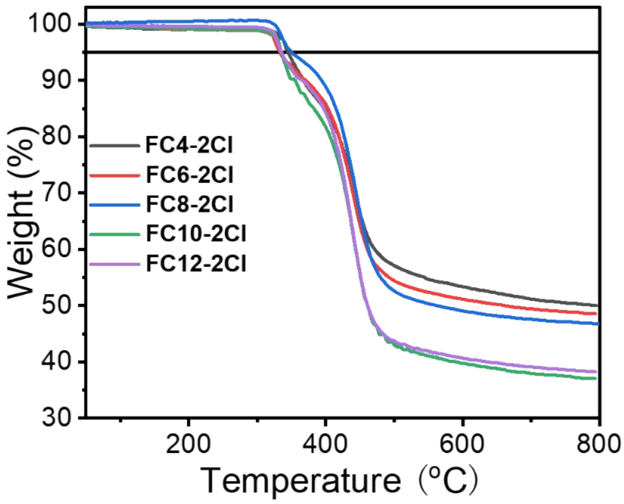

Fig. S1 The thermogravimetric analysis (TGA) plots of **FCn-2Cl**.

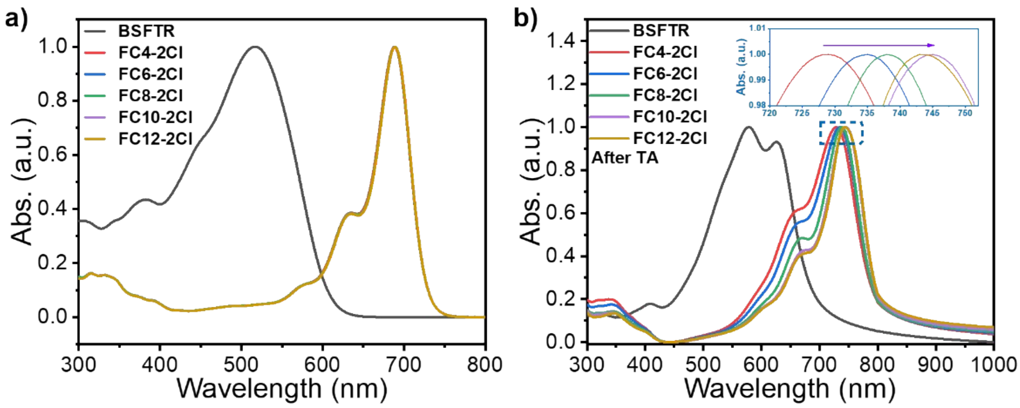

Fig. S2 Normalized UV-vis absorption spectra of BSFTR and FCn-2Cl in a) solution and b) thin films after TA 120 °C for 10 min.

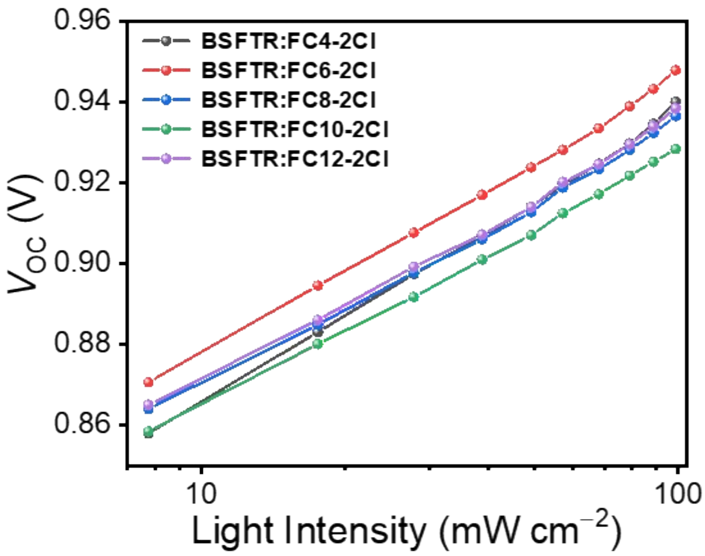

Fig. S3 Light intensity (P_{light}) dependence of V_{OC} of BSFTR:FCn-2Cl-based ASM-OSCs.

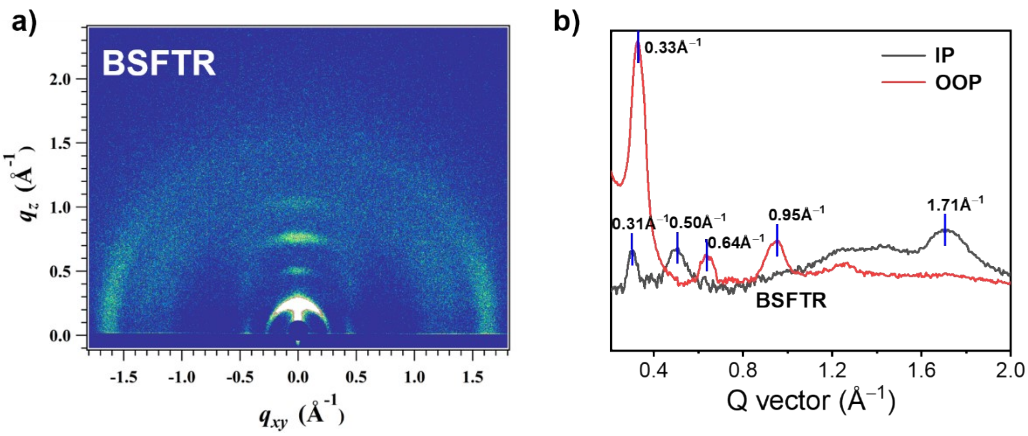

Fig. S4 a) 2D-GIWAXS pattern and b) line-cut profiles for the neat film of BSFTR.

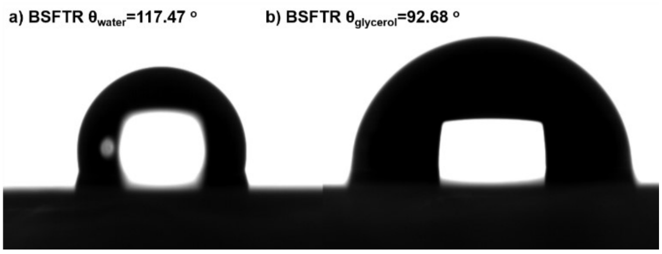

Fig. S5 a) contact angle of water and b) contact angle of glycerol on BSFTR.

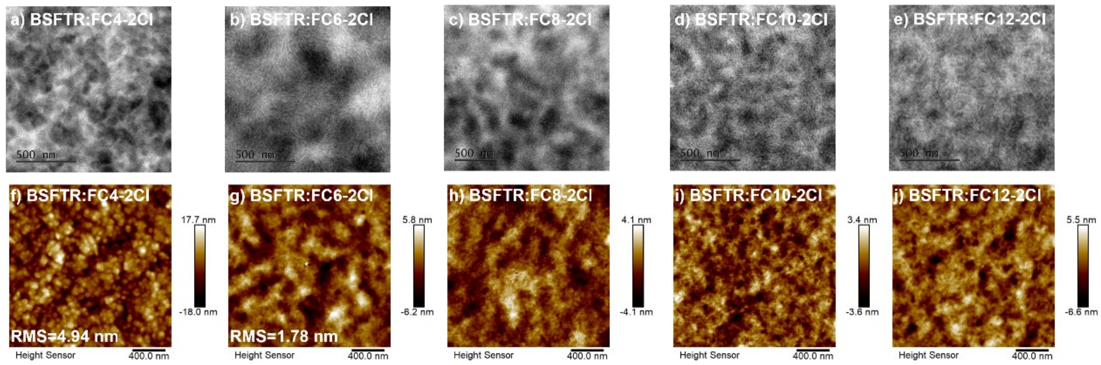

Fig. S6 a-e) TEM images and f-j) AFM images for the blend films based on **BSFTR**:**FCn-2Cl** (n=4, 6, 8, 10, 12).

Table S1. The recent work of vapor-deposition ASM-OSCs.

Active layer	V_{OC} (V)	J_{SC} (mA cm^{-2})	FF (%)	PCE (%)	Ref.
CuPc/PV	0.450	2.30	0.650	0.95	4
SubPc/F_{13}SubPc	0.940	2.10	0.490	0.96	5
SubNc/F_{13}SubPc	0.700	2.40	0.370	0.63	
AlPcCl/F_{13}SubPc	0.660	0.53	0.350	0.12	
CuPc/F_{13}SubPc	0.270	0.27	0.240	0.02	
5cene/F_{13}SubPc	0.090	1.20	0.330	0.03	
SubPc/F_{12}SubPc	0.710	2.20	0.340	0.52	
AlPcCl/F_{12}SubPc	0.600	0.99	0.320	0.19	
CuPc/F_{12}SubPc	0.160	0.53	0.290	0.02	
SubPc/C_{60}	0.920	5.40	0.610	3.00	
SubNc/C_{60}	0.790	6.50	0.490	2.50	
AlPcCl/C_{60}	0.640	3.30	0.480	1.00	
CuPc/C_{60}	0.440	3.70	0.610	1.00	
5cene/C_{60}	0.350	3.10	0.530	0.58	
SubPc/C_{60}	1.090	4.90	0.610	3.30	6
SubPc/FSubPcDimer	0.960	5.10	0.240	1.20	
FSubPcDimer/SubPc	0.890	5.80	0.480	2.50	
SubPc/FSubPcDimer/C_{60}	0.950	7.80	0.540	4.00	
SubPc/C_{60}	1.100	5.03	0.530	2.97	7
SubPc/F_3-SubPc	1.100	0.83	0.220	0.19	
SubPc/F_6-SubPc	1.220	1.56	0.430	0.80	
SubPc/Cl_6-SubPc	1.310	3.53	0.580	2.68	
ZnPc/C_{60}	0.460	14.10	0.549	3.51	8
α-6T/C_{60}	0.420	4.56	0.546	1.03	9
α-6T/SubPc	1.090	7.46	0.579	4.69	
α-6T/SubNc	0.940	12.04	0.539	6.02	
α-6T/SubNc/SubPc	0.960	14.55	0.610	8.40	
DPPT:C_{60}	0.950	5.55	0.290	1.55	10
DPPT/DPPT:C_{60}	0.960	5.78	0.380	2.11	
DPPT/DPPT:C_{70}	0.960	8.09	0.340	2.63	
DTPT/DTPT:C_{70}	0.850	6.40	0.340	1.86	
1-NPPT/1-NPPT:C_{70}	0.970	3.55	0.260	0.90	
DPPT:C_{70}/C_{70}	0.980	9.05	0.400	3.52	
DTPT:C_{70}/C_{70}	0.760	6.27	0.360	1.72	
1-NPPT:C_{70}/C_{70}	0.870	5.64	0.300	1.48	
BBTBDTM/C_{60} (PHJ)	0.910	1.23	0.350	0.39	11
BBTBDTM/C_{60} (PMHJ)	0.700	4.56	0.470	1.49	

Table S2. The recent work of solution-processed ASM-OSCs.

Active layer	V_{OC} (V)	J_{SC} (mA cm^{-2})	FF (%)	PCE (%)	Ref.
DCAE7T:$PC_{61}BM$	0.880	9.94	0.510	4.46	12
DCAEH7T:$PC_{61}BM$	0.930	9.91	0.491	4.52	
DCAO7T:$PC_{61}BM$	0.860	10.74	0.550	5.08	
DRCN4T:$PC_{71}BM$	0.900	0.70	0.380	0.24	13
DRCN5T:$PC_{71}BM$	0.920	15.66	0.680	10.08	
DRCN6T:$PC_{71}BM$	0.920	11.45	0.580	6.33	
DRCN7T:$PC_{71}BM$	0.900	14.77	0.680	9.30	
DRCN8T:$PC_{71}BM$	0.860	10.80	0.680	6.50	
DRCN9T:$PC_{71}BM$	0.810	13.77	0.680	7.86	
DCAO3T(BDT)3T:$PC_{61}BM$	0.930	9.77	0.599	5.44	14
BTR:$PC_{71}BM$	0.900	13.90	0.740	9.30	15
BTR:Y6	0.850	22.25	0.564	10.67	16
BTR-Cl:Y6	0.860	24.17	0.655	13.61	
B1:BO-4Cl	0.830	25.27	0.730	15.30	17
ZR1:Y6	0.861	24.34	0.684	14.34	18
ZR1:IDIC-4Cl	0.776	18.27	0.680	9.64	
BSFTR:Y6	0.850	23.16	0.697	13.69	19
BSFTR:FO-2Cl	0.885	22.01	0.784	15.27	20
BSFTR:FO-EH-2Cl	0.876	22.39	0.804	15.78	
C8-C-F:F-2Cl	0.936	17.71	0.733	12.15	21
C8-C-F:FO-2Cl	0.906	20.08	0.765	13.91	
M-PhS:BTP-eC9	0.840	25.40	0.756	16.20	22
P-PhS:BTP-eC9	0.880	21.60	0.626	11.90	
B1:BO-4Cl:Y7	0.836	25.52	0.763	16.28	23
B1:BO-2Cl:BO-4Cl	0.840	25.31	0.780	17.00	24

Table S3. Summary of the GIWAXS parameters for the neat films of FCn-2Cl (n=4, 6, 8, 10, 12).

Aceeptor	q_z (010) (Å^{-1})^a	FWHM (Å^{-1})^b	d_{010} (Å)	CCL (Å)^c
FC4-2Cl	1.77	0.397	3.55	14.24
FC6-2Cl	1.80	0.230	3.49	24.59
FC8-2Cl	1.81	0.184	3.47	30.73
FC10-2Cl	1.82	0.183	3.45	30.90
FC12-2Cl	1.83	0.160	3.43	35.34

^{a}The (010) diffraction peak in the OOP direction; ^{b}Full-width at half-maximum by Gaussian fitting; ^{c}CCL estimated from Scherrer's equation (CCL=2πk/FWHM).

Table S4. Photovoltaic performance of the solar cells based on BSFTR:FC4-2Cl blend films with different D:A ration under illumination of AM 1.5 G, 100 mW cm $^{-2}$.

D:A	V_{OC} (V)	J_{SC} (mA cm^{-2})	FF (%)	PCE (%)
1:0.6	0.935	11.42	0.651	6.95
1:0.8	0.932	11.60	0.684	7.39
1:1	0.928	11.22	0.681	7.09

Table S5. Photovoltaic performance of the solar cells based on BSFTR:FC4-2Cl (1:0.8, *w*/*w*) blend films with different DIO contents under illumination of AM 1.5 G, 100 mW cm $^{-2}$.

V%	V_{OC} (V)	J_{SC} (mA cm^{-2})	FF (%)	PCE (%)
none	0.939	11.34	0.696	7.41
0.3	0.937	10.67	0.691	6.90
0.5	0.910	7.89	0.651	4.67
0.7	0.900	7.51	0.637	4.31

Table S6. Photovoltaic performance of the solar cells based on BSFTR:FC4-2Cl (1:0.8, *w*/*w*) blend films with different TA temperatures under illumination of AM 1.5 G, 100 mW cm $^{-2}$.

TA (°C)	V_{OC} (V)	J_{SC} (mA cm^{-2})	FF (%)	PCE (%)
0	0.957	7.22	0.541	3.74
110	0.951	10.82	0.696	7.16
120	0.948	11.56	0.696	7.48
130	0.930	11.94	0.653	7.24

Table S7. Photovoltaic performance of the solar cells based on BSFTR:FC6-2Cl blend films with different D:A ration under illumination of AM 1.5 G, 100 mW cm $^{-2}$.

D:A	V_{OC} (V)	J_{SC} (mA cm^{-2})	FF (%)	PCE (%)
1:0.6	0.938	13.10	0.677	8.32
1:0.8	0.935	13.29	0.692	8.61
1:1	0.929	13.60	0.675	8.43

Table S8. Photovoltaic performance of the solar cells based on BSFTR:FC6-2Cl (1:0.8, *w*/*w*) blend films with different DIO contents under illumination of AM 1.5 G, 100 mW cm $^{-2}$.

V%	V_{OC} (V)	J_{SC} (mA cm^{-2})	FF (%)	PCE (%)
none	0.945	13.96	0.693	9.14
0.3	0.881	13.86	0.740	9.04
0.5	0.880	11.97	0.687	7.24
0.7	0.879	9.43	0.643	5.33

Table S9. Photovoltaic performance of the solar cells based on BSFTR:FC6-2Cl (1:0.8, *w*/*w*) blend films with different TA temperatures under illumination of AM 1.5 G, 100 mW cm $^{-2}$.

TA (°C)	V_{OC} (V)	J_{SC} (mA cm^{-2})	FF (%)	PCE (%)
0	0.961	5.04	0.315	1.52
110	0.957	13.92	0.621	8.24
120	0.949	14.77	0.703	9.85
130	0.922	13.70	0.651	8.23

Table S10. Photovoltaic performance of the solar cells based on BSFTR:FC8-2Cl blend films with different D:A ration under illumination of AM 1.5 G, 100 mW cm $^{-2}$.

D:A	V_{OC} (V)	J_{SC} (mA cm^{-2})	FF (%)	PCE (%)
1:0.6	0.931	15.95	0.672	9.97
1:0.8	0.934	16.69	0.717	11.27
1:1	0.925	17.05	0.676	10.78

Table S11. Photovoltaic performance of the solar cells based on BSFTR:FC8-2Cl (1:0.8, *w*/*w*) blend films with different DIO contents under illumination of AM 1.5 G, 100 mW cm $^{-2}$.

V%	V_{OC} (V)	J_{SC} (mA cm^{-2})	FF (%)	PCE (%)
none	0.942	18.08	0.693	11.81
0.3	0.932	16.40	0.731	11.18
0.5	0.918	9.09	0.617	5.15
0.7	0.909	9.75	0.530	4.70

Table S12. Photovoltaic performance of the solar cells based on BSFTR:FC8-2Cl (1:0.8, *w*/*w*) blend films with different TA temperatures under illumination of AM 1.5 G, 100 mW cm $^{-2}$.

TA (°C)	V_{OC} (V)	J_{SC} (mA cm^{-2})	FF (%)	PCE (%)
0	0.954	5.16	0.317	1.56
110	0.946	17.13	0.664	10.73
120	0.942	18.05	0.729	11.99
130	0.938	18.11	0.686	11.66

Table S13. Photovoltaic performance of the solar cells based on BSFTR:FC10-2Cl blend films with different D:A ration under illumination of AM 1.5 G, 100 mW cm $^{-2}$.

D:A	V_{OC} (V)	J_{SC} (mA cm^{-2})	FF (%)	PCE (%)
1:0.6	0.932	17.10	0.696	11.05
1:0.8	0.933	17.34	0.723	11.71
1:1	0.918	17.10	0.696	10.93

Table S14. Photovoltaic performance of the solar cells based on BSFTR:FC10-2Cl (1:0.8, *w*/*w*) blend films with different DIO contents under illumination of AM 1.5 G, 100 mW cm $^{-2}$.

V%	V_{OC} (V)	J_{SC} (mA cm^{-2})	FF (%)	PCE (%)
none	0.935	17.82	0.728	12.12
0.3	0.932	16.84	0.745	11.69
0.5	0.951	12.16	0.664	7.69
0.7	0.946	10.34	0.561	5.48

Table S15. Photovoltaic performance of the solar cells based on BSFTR:FC10-2Cl (1:0.8, *w*/*w*) blend films with different TA temperatures under illumination of AM 1.5 G, 100 mW cm $^{-2}$.

TA (°C)	V_{OC} (V)	J_{SC} (mA cm^{-2})	FF (%)	PCE (%)
0	0.953	5.54	0.323	1.71
110	0.944	17.28	0.659	10.75
120	0.938	18.53	0.738	12.54
130	0.928	18.00	0.690	11.53

Table S16. Photovoltaic performance of the solar cells based on BSFTR:FC12-2Cl blend films with different D:A ration under illumination of AM 1.5 G, 100 mW cm $^{-2}$.

D:A	V_{OC} (V)	J_{SC} (mA cm^{-2})	FF (%)	PCE (%)
1:0.6	0.933	15.06	0.712	10.01
1:0.8	0.935	16.44	0.730	11.18
1:1	0.925	16.46	0.684	10.38

Table S17. Photovoltaic performance of the solar cells based on BSFTR:FC12-2Cl (1:0.8, *w*/*w*) blend films with different DIO contents under illumination of AM 1.5 G, 100 mW cm $^{-2}$.

V%	V_{OC} (V)	J_{SC} (mA cm^{-2})	FF (%)	PCE (%)
none	0.941	16.62	0.745	11.37
0.3	0.942	14.15	0.701	9.34
0.5	0.953	10.82	0.637	6.57
0.7	0.946	10.34	0.561	5.48

Table S18. Photovoltaic performance of the solar cells based on BSFTR:FC12-2Cl (1:0.8, *w*/*w*) blend films with different TA temperatures under illumination of AM 1.5 G, 100 mW cm $^{-2}$.

TA (°C)	V_{OC} (V)	J_{SC} (mA cm^{-2})	FF (%)	PCE (%)
0	0.986	9.33	0.503	4.63
110	0.944	16.16	0.732	10.88
120	0.944	16.83	0.750	11.47
130	0.924	16.49	0.698	10.64

Table S19. The detailed data of physical dynamic characterizations for **BSFTR**:**FCn-2Cl**-based devices.

Acceptors	P_{diss}	P_{coll}	α	n	TPV (ms)	TPC (μs)	μ_h (10^{-4} cm^2 V^{-1} s^{-1})	μ_e (10^{-4} cm^2 V^{-1} s^{-1})	μ_h/μ_e
FC4-2Cl	88%	71%	0.98	1.34	19.1	0.359	1.35	1.08	1.25
FC6-2Cl	92%	74%	0.98	1.26	21.1	0.332	1.48	1.26	1.17
FC8-2Cl	96%	83%	0.99	1.20	29.0	0.318	1.75	1.60	1.09
FC10-2Cl	96%	84%	0.99	1.17	30.4	0.277	1.79	1.70	1.05
FC12-2Cl	94%	82%	0.99	1.21	24.6	0.324	1.52	1.36	1.12

Table S20. The χ values calculated from surface tensions.

Neat films	θ_{water} [°]	$\theta_{glycerol}$ [°]	γ [mN m^{-1}]	χ
BSFTR	117.47	92.68	-	-
FC4-2Cl	105.93	77.20	46.60	2.63
FC6-2Cl	109.46	79.73	39.23	1.12
FC8-2Cl	110.78	80.41	38.43	0.99
FC10-2Cl	114.87	82.53	35.69	0.59
FC12-2Cl	118.77	80.71	35.14	0.52

5. NMR and HR-MS

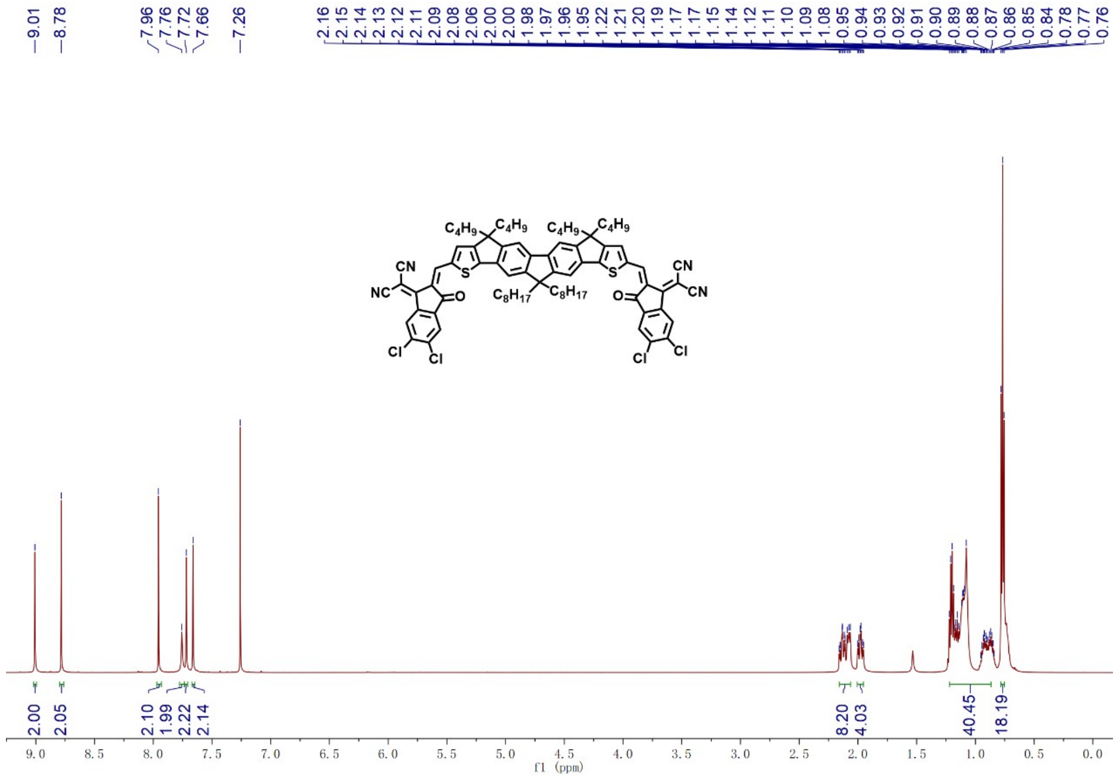

Fig. S7 ^{1}H NMR spectrum of **FC4-2Cl** in $CDCl_3$.

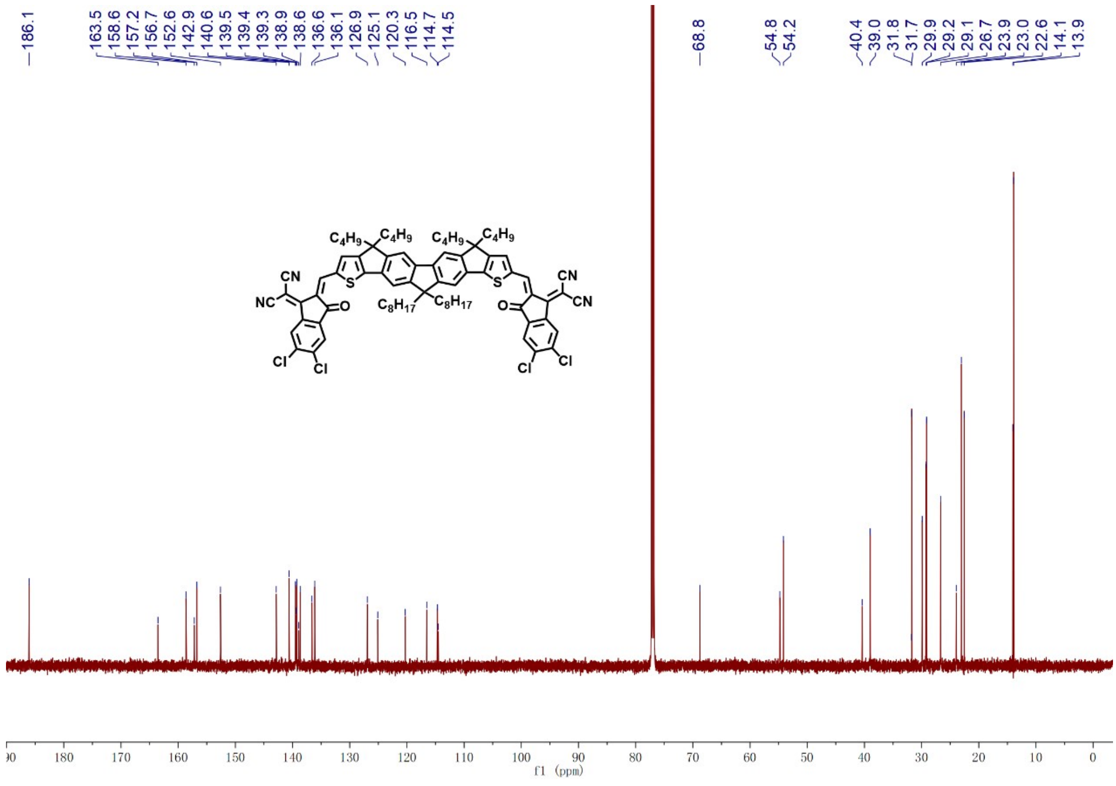

Fig. S8 ^{13}C NMR spectrum of **FC4-2Cl** in $CDCl_3$.

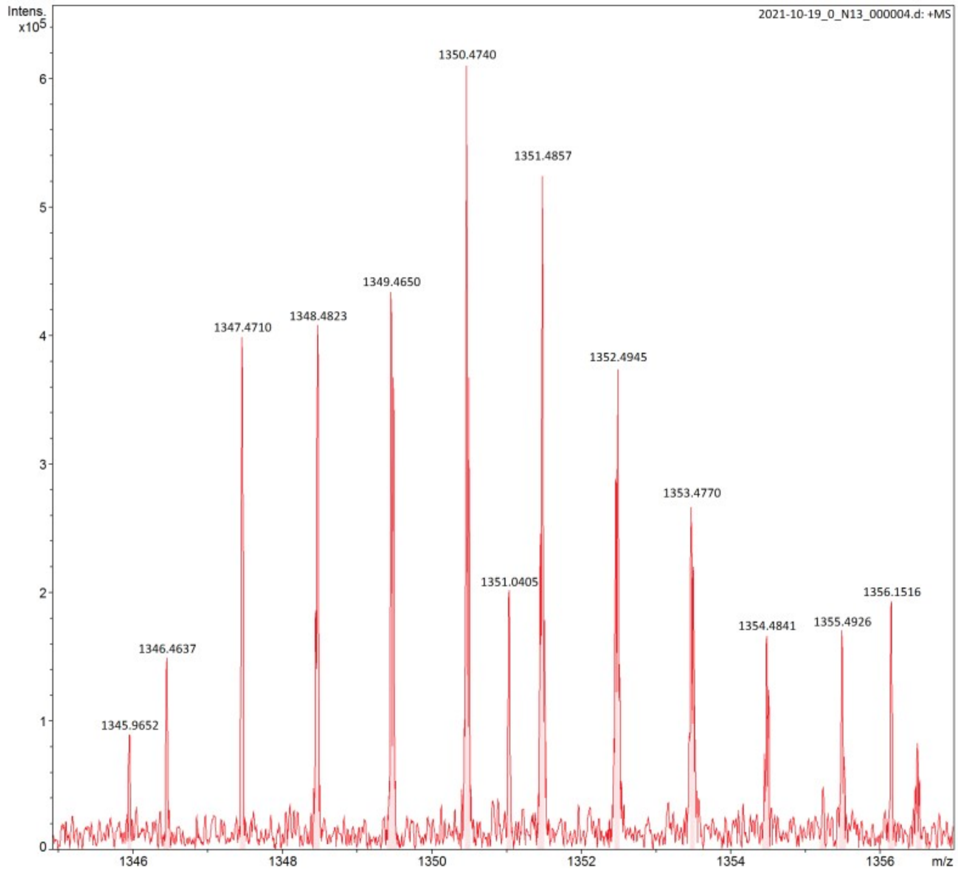

Fig. S9 HR-MS spectrum of **FC4-2Cl**.

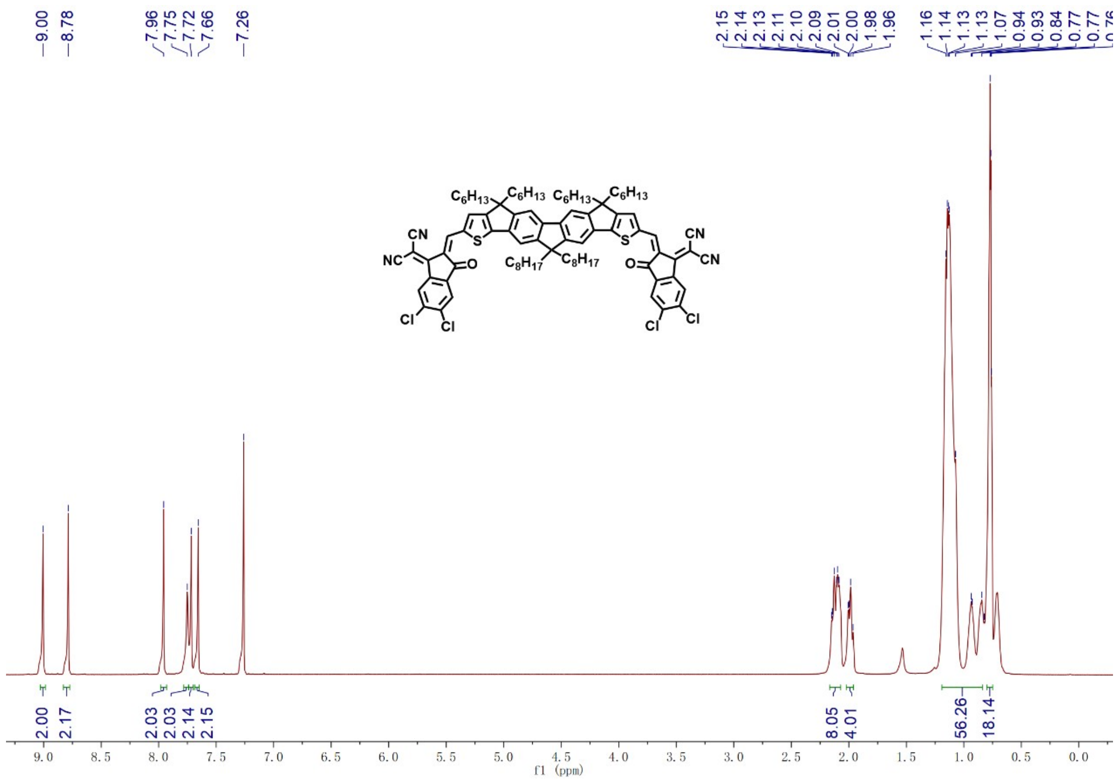

Fig. S10 ^{1}H NMR spectrum of **FC6-2Cl** in $CDCl_3$.

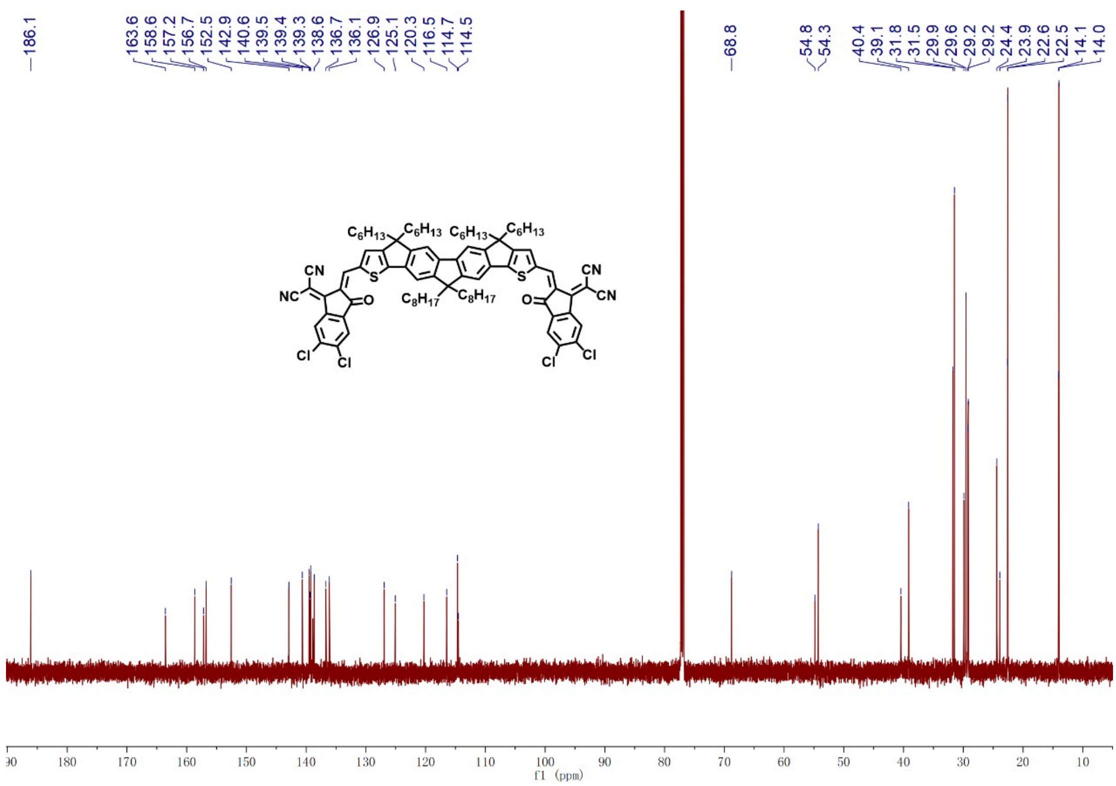

Fig. S11 ^{13}C NMR spectrum of **FC6-2Cl** in $CDCl_3$.

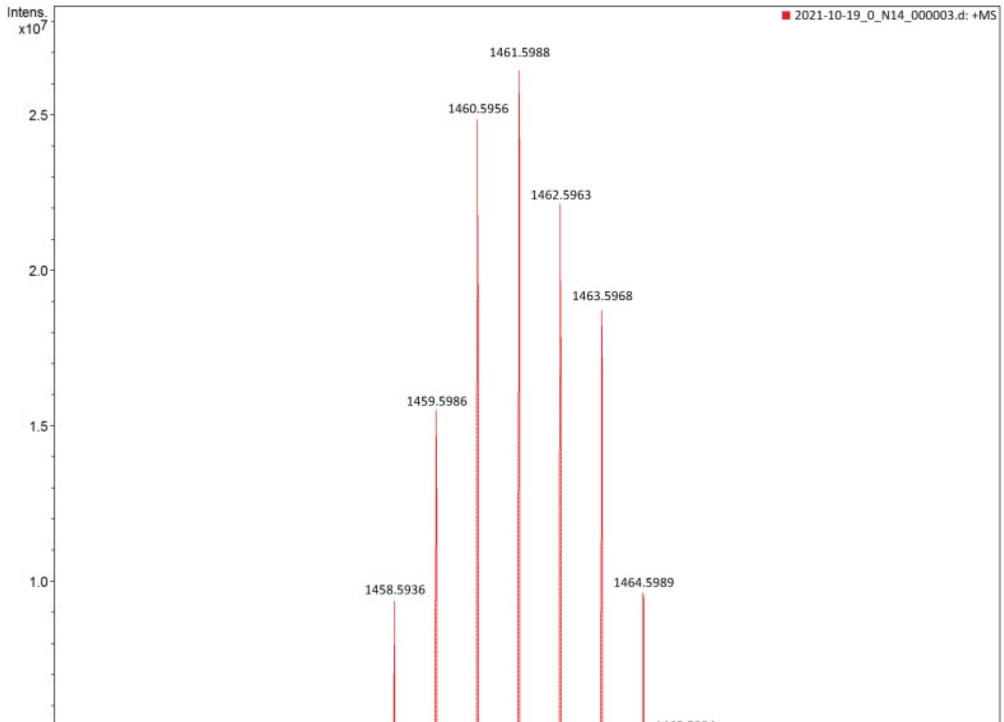

Fig. S12 HR-MS spectrum of **FC6-2Cl**.

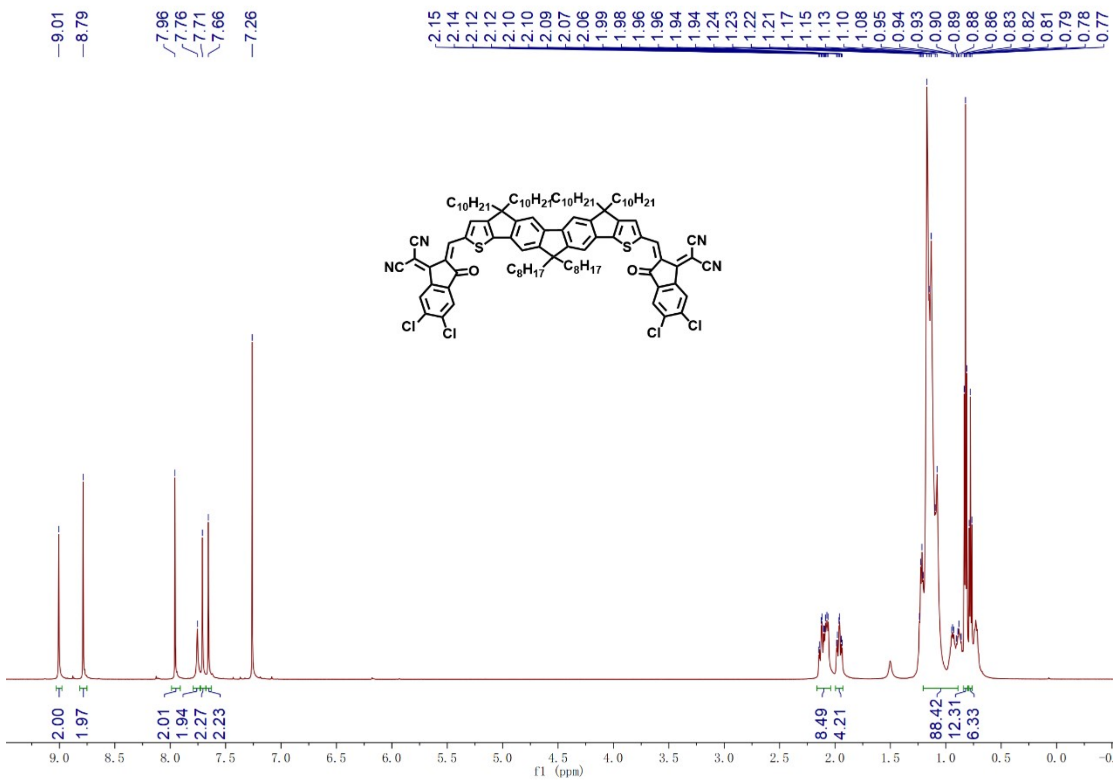

Fig. S13 ^{1}H NMR spectrum of **FC10-2Cl** in $CDCl_3$.

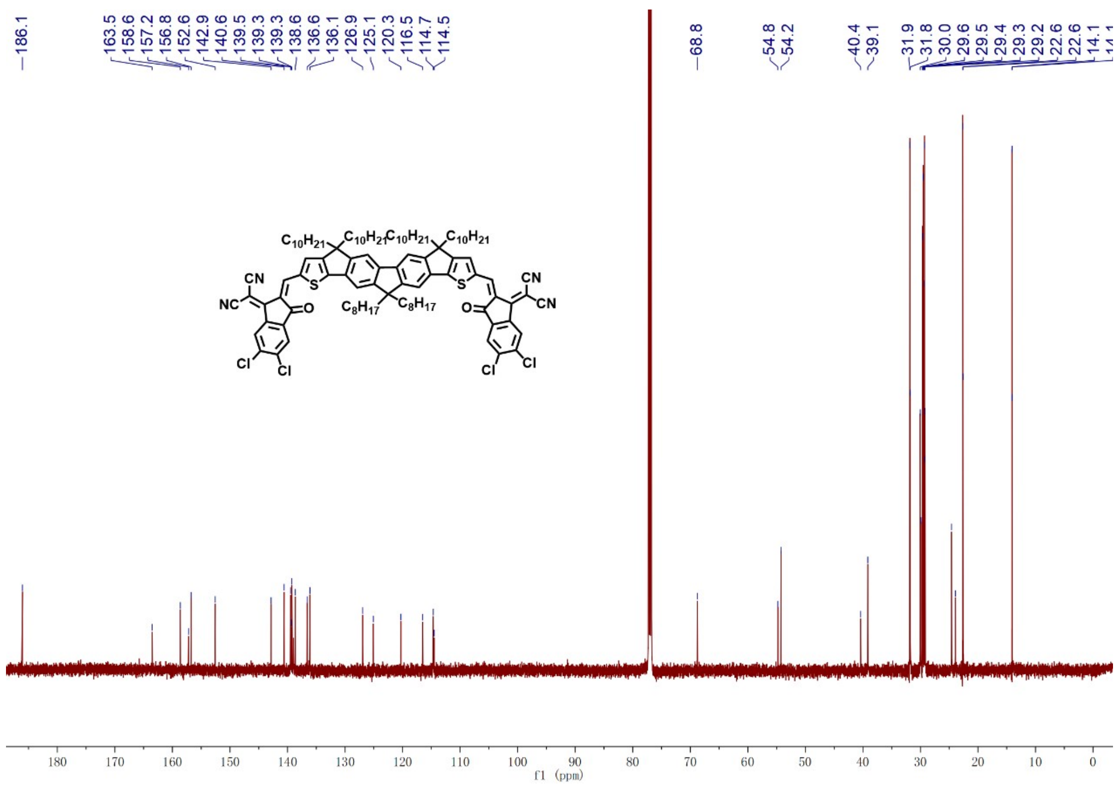

Fig. S14 ^{13}C NMR spectrum of **FC10-2Cl** in $CDCl_3$.

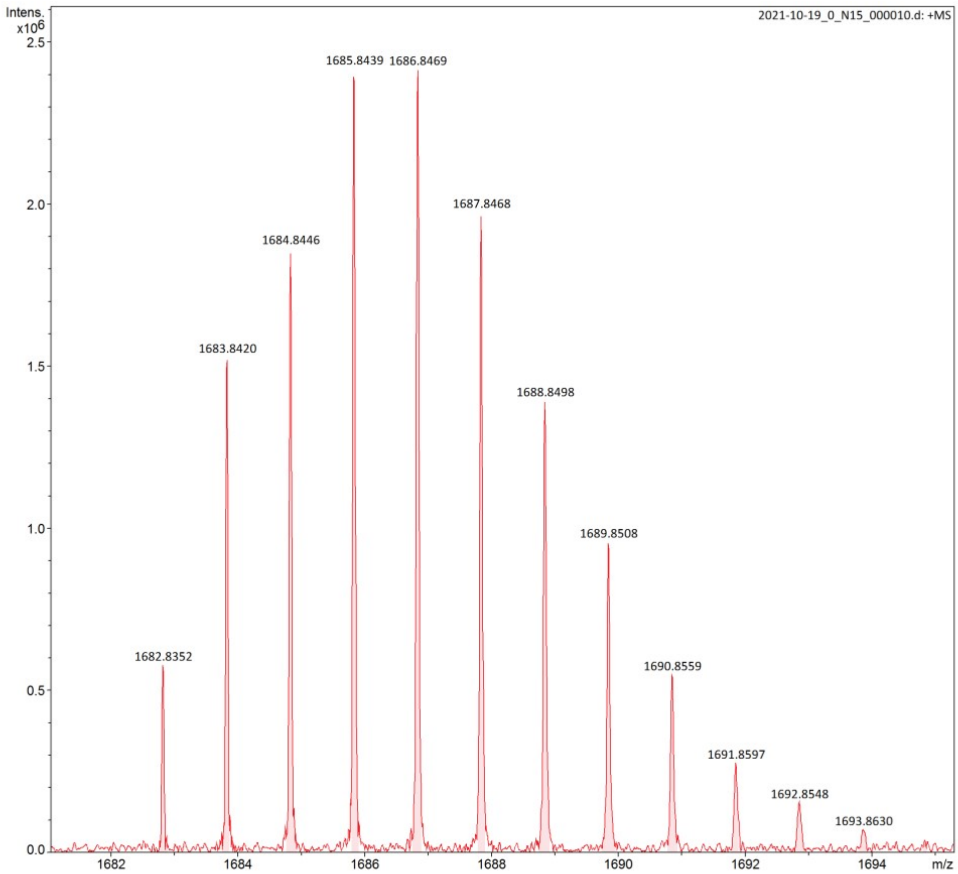

Fig. S15 HR-MS spectrum of **FC10-2Cl**.

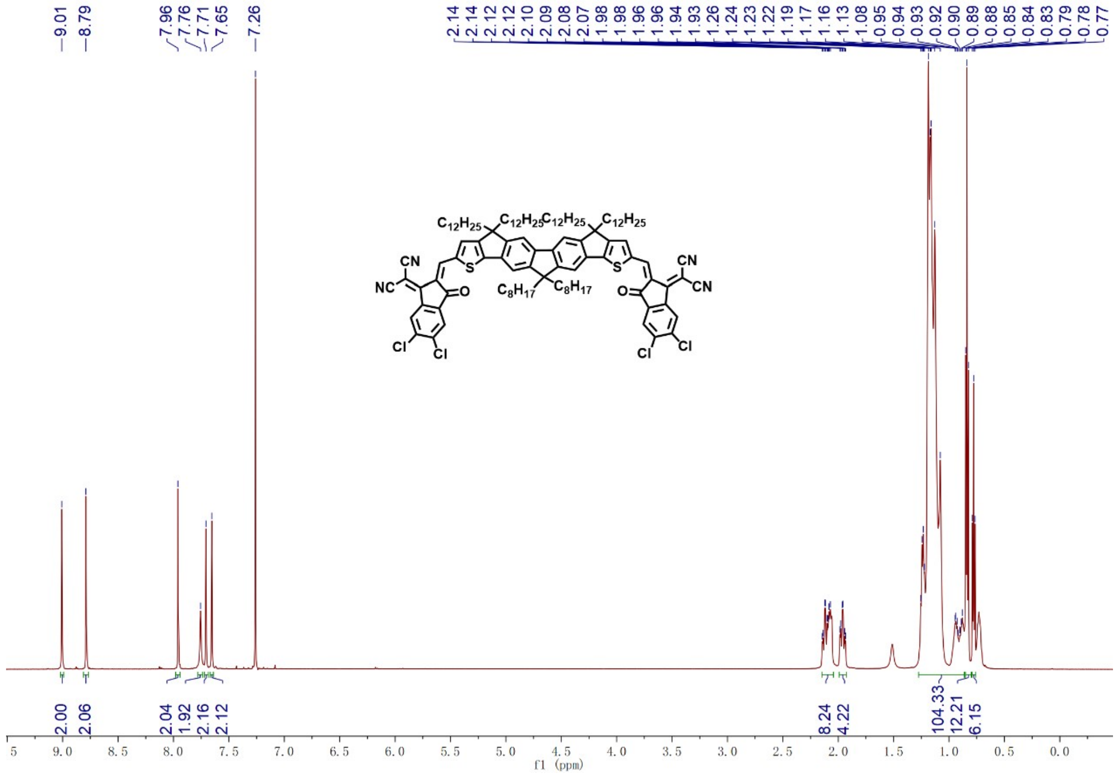

Fig. S16 ^{1}H NMR spectrum of **FC12-2Cl** in $CDCl_3$.

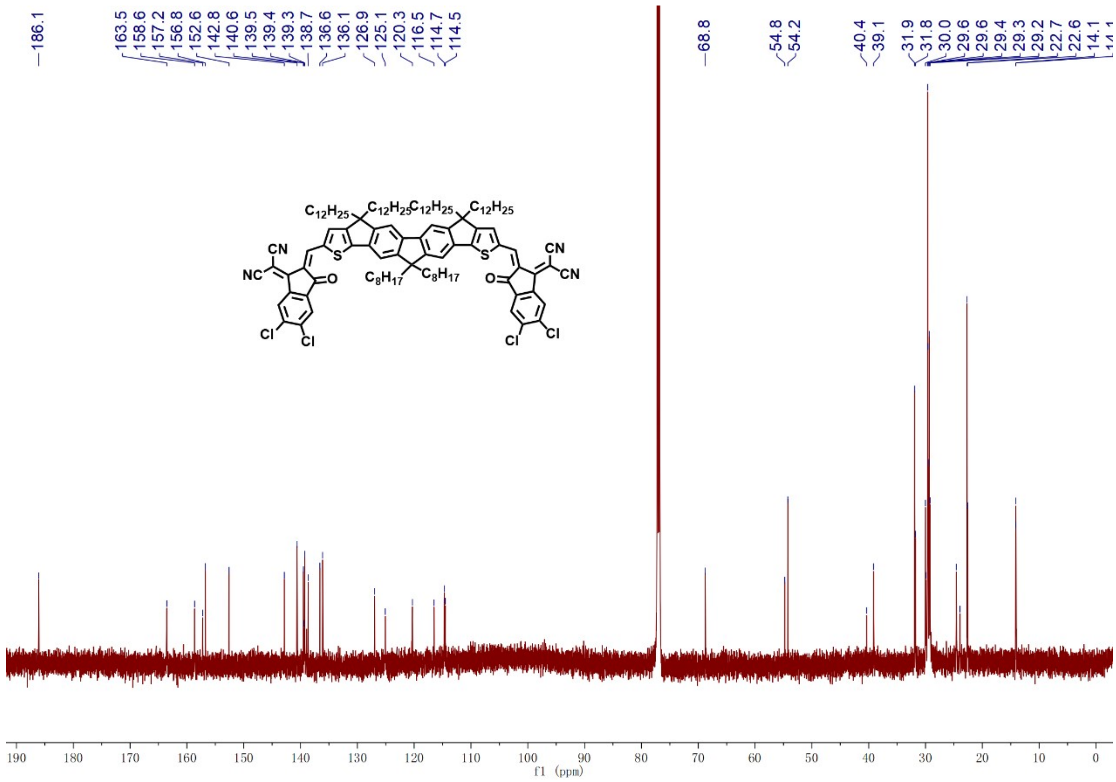

Fig. S17 ^{13}C NMR spectrum of **FC12-2Cl** in $CDCl_3$.

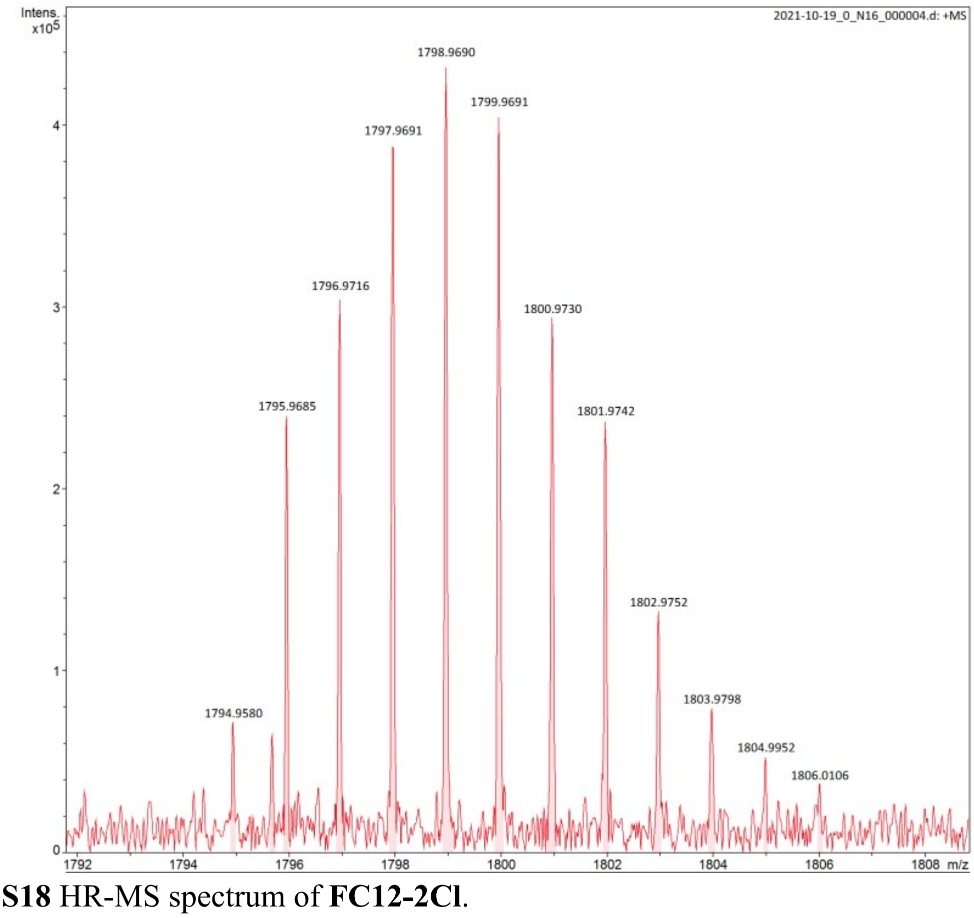

Fig. S18 HR-MS spectrum of **FC12-2Cl**.

6. Reference

1. C.-Y. Chang; Y.-J. Cheng; S.-H. Hung; J.-S. Wu; W.-S. Kao; C.-H. Lee, C.-S. Hsu, *Adv Mater* 2012, **24**, 549-553.
2. N. L. Qiu; H. J. Zhang; X. J. Wan; C. X. Li; X. Ke; H. R. Feng; B. Kan; H. T. Zhang; Q. Zhang; Y. Lu, Y. S. Chen, *Adv Mater* 2017, **29**, 1604964.
3. Y. Wang; Y. Wang; B. Kan; X. Ke; X. Wan; C. Li, Y. Chen, *Adv Energy Mater* 2018, **8**, 1802021.
4. C. W. Tang, *Appl Phys Lett* 1986, **48**, 183-185.
5. H. Gommans; T. Aernouts; B. Verreet; P. Heremans; A. Medina; C. G. Claessens, T. Torres, *Adv Funct Mater* 2009, **19**, 3435-3439.
6. B. Verreet; B. P. Rand; D. Cheyns; A. Hadipour; T. Aernouts; P. Heremans; A. Medina; C. G. Claessens, T. Torres, *Adv Energy Mater* 2011, **1**, 565-568.
7. P. Sullivan; A. Duraud; l. Hancox; N. Beaumont; G. Mirri; J. H. R. Tucker; R. A. Hatton; M. Shipman, T. S. Jones, *Adv Energy Mater* 2011, **1**, 352-355.
8. J. Lee; D. Park; I. Heo, S. Yim, *Mater Res Bull* 2014, **58**, 132-135.
9. K. Cnops; B. P. Rand; D. Cheyns; B. Verreet; M. A. Empl, P. Heremans, *Nat Commun* 2014, **5**, 3406.
10. K.-W. Chen; C.-W. Huang; S.-Y. Lin; Y.-H. Liu; T. Chatterjee; W.-Y. Hung; S.-W. Liu, K.-T. Wong, *Org Electron* 2015, **26**, 319-326.
11. D. Park; I. H. Jung; S.-Y. Jang, S. Yim, *Macromol Res* 2019, **27**, 444-447.
12. Y. Liu; X. Wan; F. Wang; J. Zhou; G. Long; J. Tian; J. You; Y. Yang, Y. Chen, *Adv Energy Mater* 2011, **1**, 771-775.
13. B. Kan; M. Li; Q. Zhang; F. Liu; X. Wan; Y. Wang; W. Ni; G. Long; X. Yang; H. Feng; Y. Zuo; M. Zhang; F. Huang; Y. Cao; T. P. Russell, Y. Chen, *J Am Chem Soc* 2015, **137**, 3886-3893.
14. Y. Liu; X. Wan; F. Wang; J. Zhou; G. Long; J. Tian, Y. Chen, *Adv Mater* 2011, **23**, 5387-5391.
15. K. Sun; Z. Xiao; S. Lu; W. Zajaczkowski; W. Pisula; E. Hanssen; J. M. White; R. M. Williamson; J. Subbiah; J. Ouyang; A. B. Holmes; W. W. H. Wong, D. J. Jones, *Nat Commun* 2015, **6**,
16. H. Chen; D. Hu; Q. Yang; J. Gao; J. Fu; K. Yang; H. He; S. Chen; Z. Kan; T. Duan; C. Yang; J. Ouyang; Z. Xiao; K. Sun, S. Lu, *Joule* 2019, **3**, 3034-3047.
17. J. Qin; C. An; J. Zhang; K. Ma; Y. Yang; T. Zhang; S. Li; K. Xian; Y. Cui; Y. Tang; W. Ma; H. Yao; S. Zhang; B. Xu; C. He, J. Hou, *Sci China Mater* 2020, **63**, 1142-1150.
18. R. Zhou; Z. Jiang; C. Yang; J. Yu; J. Feng; M. A. Adil; D. Deng; W. Zou; J. Zhang; K. Lu; W. Ma; F. Gao, Z. Wei, *Nat Commun* 2019, **10**,
19. Q. Yue; H. Wu; Z. Zhou; M. Zhang; F. Liu, X. Zhu, *Adv Mater* 2019, **31**, e1904283.
20. L. Meng; M. Li; G. Lu; Z. Shen; S. Wu; H. Liang; Z. Li; G. Lu; Z. Yao; C. Li; X. Wan, Y. Chen, *Small* 2022, e2201400.
21. L. Meng; S. Wu; X. Wan; Z. Shen; M. Li; Y. Yang; J. Wang; G. Lu; Z. Ma; Z. Yao; C. Li, Y. Chen, *Chem Mater* 2022, **34**, 3168-3177.

22. L. Zhang; X. Zhu; D. Deng; Z. Wang; Z. Zhang; Y. Li; J. Zhang; K. Lv; L. Liu; X. Zhang; H. Zhou; H. Ade, Z. Wei, *Adv Mater* 2022, **34**, e2106316.
23. M. Jiang; H. Bai; H. Zhi; L. Yan; H. Y. Woo; L. Tong; J. Wang; F. Zhang, Q. An, *Energy Environ Sci* 2021, **14**, 3945-3953.
24. J. Qin; Z. Chen; P. Bi; Y. Yang; J. Zhang; Z. Huang; Z. Wei; C. An; H. Yao; X. Hao; T. Zhang; Y. Cui; L. Hong; C. Liu; Y. Zu; C. He, J. Hou, *Energy Environ Sci* 2021, **14**, 5903-5910.